Revista Fuentes: El Reventón Energético
Vol. 14 Nº 2 de 2016 - Jul/Dic - pp 85/97

STUDY OF CONDUCTIVITY LOSS DUE TO PROPPANT EMBEDMENT ON SHALE PLAYS BY NUMERICAL SIMULATION

Kristhian Leandro Peña Cerón[1]*, Luis Carlos Prada Socha[2], José Carlos Cárdenas Montes[3]

*To whom correspondence should be addressed

ABSTRACT

Proppant embedment is inherent in reservoir fracking stimulation, this phenomenon occurs when the in-situ stresses are applied to the proppants surface causing their incrustation into the formation. Proppant embedment occasion conductivity, production and money losses, these issues are intensified in unconventional reservoir of shale plays.

This work describes geomechanical and compositional factors, which influence on embedment, as well as some embedment models. Fracture conductivity and width loss are studied by reservoir numerical simulation. The software Predict K was use to pre-select the proppant types implemented onto the simulation. The numerical simulation was carried out on a Black Oil simulator: IMEX, from the CMG suite. Embedment fractures are duplicated with a double permeability model for a gas shale play, this considering closure effective stress through permeability and porosity multipliers.

In this article were generated conductivity curves that show proppant performance with applied stress in production. Due to shale data scarcity working with the methodology of this work is convenient, the multipliers can replicate geomechanics without high computational effort. Additionally, it is shown mineralogy and geomechanics impacts on shale gas exploitation.

Keywords: Geomechanics, Hydraulic fracture, Double permeability model, Porosity multiplayer, Permeability multiplayer. Gas reservoir, Unconventional reservoir.

Estudio de la perdida de conductividad debida a empotramiento de propante en formaciones de shale mediante simulación numérica

RESUMEN

El empotramiento es inherente en la estimulación de yacimientos a través de fracturamiento hidráulico, ocurre cuando los esfuerzos en sitio son aplicados a la superficie de los propantes causando su incrustación en la formación. El empotramiento ocasiona pérdidas de conductividad producción y dinero, intensificándose en yacimientos no convencionales de formaciones de lutitas.

Este trabajo describe algunos factores composicionales y geomecánicos que influyen en el empotramiento, así como modelos matemáticos de empotramiento. Se estudia la pérdida de conductividad y ancho de fractura a través de simulación numérica. El software Predick K fue usado para pre-seleccionar los tipos de propante implementados en la simulación. La simulación numérica fue corrida en un simulador de Aceite Negro: IMEX, de la suite CMG.

1. Escuela de Ingeniería de Petróleos, Universidad Industrial de Santander (UIS), Carrera 27 calle 9, Bucaramanga, Santander, Colombia. E-mail: leandropceron@gmail.com.

2. Escuela de Ingeniería de Petróleos, Universidad Industrial de Santander (UIS), Carrera 27 calle 9, Bucaramanga, Santander, Colombia. E-mail: luiscarlosps93@gmail.com.

3. Ecopetrol S. A. – Instituto Colombiano del Petróleo (ICP), A. A. 4185 Piedecuesta, Santander, Colombia. E-mail: jose.cardenasmo@ecopetrol.com.co.

DOI: http://dx.doi.org/10.18273/revfue.v14n2-2016008

Las fracturas empotradas son simuladas con un modelo de doble permeabilidad para un yacimiento de gas de lutita, considerando el esfuerzo de cierre efectivo mediante multiplicadores de permeabilidad y porosidad.

En este artículo se generaron curvas de conductividad que muestran el desempeño del propante con esfuerzos aplicados en la producción. Debido a la escasez de datos de yacimientos de lutita, trabajar con la metodología de este trabajo es conveniente, los multiplicadores pueden replicar la geomecánica sin un alto esfuerzo computacional. Adicionalmente, se muestra los impactos de la mineralogía y geomecánica en la explotación de gas de lutita.

Palabras clave: Geomecánica, Fractura hidráulica, Modelo de doble permeabilidad, Multiplicador de porosidad, Multiplicador de permeabilidad, Yacimiento de gas, Yacimiento no convencional.

1. INTRODUCTION

Conductivity loss due to proppant embedment is presented in hydraulic fractures of fracking stimulation. The embedment appears when the minimum horizontal stress acts on the proppant material; the minimum horizontal stress is counterbalanced by a combined action of fluid pressure and a contact pressure, which exists between the fracture face and proppants. In the presence of depletion, the contact pressure raises generating material incrustation into the formation (Cui, Glover & Wust, 2014). The embedment is significant when the proppant-formation ratio of the Elastic Modulus is high and also when the reservoir formation is soft, formations with Young Moduli of their minerals under 30 GPa are considered softs (Akrad, Miskimins & Prasad, 2011).

Shale gas reservoir production depends upon hydraulic fracture conductivity by creating fractures to increase shale permeabilities of 0.1-1000 nanodarcy to permeabilities with greater magnitudes (Alexander et al., 2011). Conductivity loss generated by embedment affects production, fracture width reduction in soft formations could be up to the 40% (Lacy, Rickards & Ali, 1997) and 31% in shales (Corapcioglu, Minskimins & Prasad, 2014).

Performing laboratory activities is the ideal mean to quantify embedment, although this implies to use sophisticate instrumentation and considerable expenses, those laboratories must have special procedures to evaluate shale. Therefore, it is necessary to look for and implement methodologies that allows embedment analysis in an accessible way. Shale data is scarce, as a result the implementation of simulations have to be integral to avoid imprecisions.

Works made, for example, Cui et al. (2014) simulated only the embedment without taking into account impacts on the well/reservoir. Yu and Sepehrnoori (2013a) used the black-oil simulator IMEX of CMG to evaluate desorption effect and geomechanics in a shale gas reservoir, the geomechanics was carried out by conductivity multipliers. Yu and Sepehrnoori (2013b) added a proppant distribution analysis to their former methodology. Yu and Sepehrnoori's works did not count the initial fracture stress, neither proppant type in the stress application, whereas in this work are integrated.
This work integrate simultaneously the geomechanics and performance of different proppants through conductivity baselines given by the Predict K software (Core Laboratories). These baselines are utilised to create permeability and porosity multipliers which are put into the IMEX simulation. Result analysis is centered on the hydraulic fractures, explicitly defined, taking pressure changes and relating it to production over time and closure pressure. This accomplishment does not consider fluid retention inside proppant packs, neither flowback phenomenon in the conductivity decrease as well as diagenetic effects nor fines over proppants.

Summary of contributions:

- A review of phenomena which could influence on the embedment.
- Shows mathematical models developed to calculate proppant embedment.
- Indicates conductivity baselines from Predict-K software and establishes parameters to pre-select proppants for shale plays.
- Uses effective stress and relates it to conductivity baselines to generate permeability multipliers and subsequently porosity multipliers.
- Relates both, cumulative production to conductivity variations and volume compaction to width loss in the hydraulic fracture.
- Shows production changes led by desorption and proppant geomechanics.

2. PROPERTIES WHICH AFFECT EMBEDMENT AND MODELS TO QUANTIFY EMBEDMENT

Amongst the rock properties critical for embedment, the rock Young Modulus has an inverse relation with the embedment (Alramahi & Sundberg, 2012), in contrast with the proppant Young Modulus. Similarly, when the Poisson ratio values increase, elastic and creep embedment diminishes, total amount decreases; Poisson ratio effect on embedment is insignificant (Guo & Liu, 2012).

Effective stresses hold by proppant contribute to the appearance of embedment, cyclic stresses on proppants increment the possibility of phenomena that lessen the fracture width (Terracina, Turner, Collins, & Spillars, 2010), also embedment enlargement per cycle (Lacy, Rickards & Bilden, 1998). Weakness planes and natural fractures cause preferential indentation, the location of proppants inside the natural fractures along with applied stresses result in higher incrustation (Akrad et al., 2011) (Corapcioglu et al., 2014); proppant migration from hard to unstable zones also enables to the indentation (Corapcioglu et al., 2014).

In a different way, embedded fractures with face roughness, without aligned faces, have a major conductivity than aligned fracture faces having and no having proppants (Fredd, C., McConnell, S., Boney, C. & England, K., 2000). Even though there is not a direct relation with embedment, roughness produces a greater pressure dependence of conductivity (Kassis & Sondergeld, 2010).

Rock and fluid composition has repercussions on embedment (Akrad et al., 2011) (Corapcioglu et al., 2014), Young Modulus reduction due to fluid interaction is evident in certain rock-fluid combinations. Temperature for high Calcite content formations has negative effects as well. According to Corapcioglu et al. (2014) the re-precipitation onto the fracture faces of dissolved Carbonates can enable zones for incrustation. Embedment is larger in liquid producing formations.

Embedment Models

Huitt & McGlothlin (1958). Made a semi-empiric model taking into account the overburden, geometric parameters, proppant concentration inside the hydraulic fracture, and characteristic factors of rock for a monolayer pattern. Gao et al. (2013) derived the next equation based upon the Huitt and McGlothlin (1958) work adding the K parameter, distance amongst proppants coefficient.

$$h = \frac{1}{2} D_1\{ 1 - [1 - B (K^2 p)^{m1}]^{0.5}\} \quad (1)$$

Guo & Liu (2012). Created a model that describes embedment in two stages: Elastic (H1), instantaneous and *creep* or viscous-elastic (H2), when proppant is being slowly embedded into the rock.

$$H_1 = \frac{2\,(1-\nu^2)\,P_c{}^a}{E} \quad (2)$$

$$H_2(t) = \frac{P_c{}^a}{2}\left[\frac{t}{\eta_2} - \frac{(1-2\nu)^2}{E}\left(\frac{-E}{e^{3\eta_2}}t - 1\right)\right] \quad (3)$$

The *Equation 4* includes the net closure stress, closure stress minus pore pressure, and pressure dependence of creep deformation over time. The sum of these two determines total proppant embedment, simplifying for H1, Pc(t) = Pc(t0) initial time after the fracking.

$$h = \frac{2P_c(t)(1-\nu^2)a}{E} + \frac{a}{2\eta_2}\left(1+\frac{(1-2\nu)^2}{3}\right)\int_0^t P_c(t)dt \quad (4)$$

Gao *et al.* (2013). Developed a model to calculate proppant embedment, proppant deformation and fracture aperture applicable to sandstone formations poorly consolidated, shale rock and coalbed methane. The model considers geomechanic and geometric parameters of rock and proppant. Furthermore, they established equations for monolayer and multilayer proppant distribution.

$$\alpha = 1.04 D_1 (K^2 p C_E)^{\frac{2}{3}} + D_2 \frac{p}{E_2} \quad (5)$$

$$\beta = 1.04 D_1 \left(K^2 p \frac{1-\nu_1{}^2}{E_1}\right)^{\frac{2}{3}} \quad (6)$$

$$h = 1.04 D_1 (K^2 p)^{\frac{2}{3}}\left[\left(\frac{1-\nu_1{}^2}{E_1} + \frac{1-\nu_2{}^2}{E_2}\right)^{\frac{2}{3}} - \left(\frac{1-\nu_1{}^2}{E_1}\right)^{\frac{2}{3}}\right] + D_2 \frac{p}{E_2} \quad (7)$$

α is the fracture aperture change (half of the value), β is the proppant deformation, and h the embedment. *Equiations 6, 7* are the same for monolayer and multilayer models, the difference resides in the range of values for h, which for the monolayer model start in zero to half of the proppant diameter, whilst the multilayer model have values between zero to half of the initial fracture width. *Equation 8* represent for the multilayer model and the *Equation 9* adds two correction factors to adjust the embedment for this model.

$$\alpha = 1.04D(K^2p)^{\frac{2}{3}}\left\{\left(\frac{1-\nu_1^2}{E_1}\right)^{\frac{2}{3}} + \frac{D_1}{D}\left[\left(\frac{1-\nu_1^2}{E_1}+\frac{1-\nu_2^2}{E_2}\right)^{\frac{2}{3}}-\left(\frac{1-\nu_1^2}{E_1}\right)^{\frac{2}{3}}\right]\right\} \quad (8)$$

$$h = b_0 + b_1\left\{1.04D_1(K^2p)^{\frac{2}{3}}\left[\left(\frac{1-\nu_1^2}{E_1}+\frac{1-\nu_2^2}{E_2}\right)^{\frac{2}{3}}-\left(\frac{1-\nu_1^2}{E_1}\right)^{\frac{2}{3}}\right]+D_2\frac{p}{E_2}\right\} \quad (9)$$

3. PROPPANT SELECTION AND IMPLEMENTATION OF THE SIMULATION MODEL

Proppant selection. Commonly in shale reservoirs are used sand proppants, particularly sizes of 100 mesh. When conductivity is important 40/70, 30/50 and 20/40 mesh size are used, although field observations link these proppants with downward propagation in brittle shales containing no frac barriers. Proppant alternatives are: Bauxite with small mesh, synthetic medium strength proppants (ceramics) and light weight ceramic proppants (LWC) (King, 2010).

Areal proppant concentration has to be high, for soft formations 3lbm/ft2 or higher (Lacy et al., 1998), and as similarly Fredd et al. (2000) mentioned, it has to be a minimum value of 1lbm/ft2. The Predict-K software of Core Laboratories allows to calculate concentration base upon hydraulic fracture width, 0.01 ft programmed in this study. The concentration, which ranges from 1.0811 lbm/ft2 to 1.2 lbm/ft2, in accordance with the proppant types pre-selected. Predict-K considers rock Young Modulus, fluid type (Gas or Oil), reservoir temperature and number of cycles along with proppant properties in the conductivity baseline calculations. In this work was provided: Young's Modulus, 24 Gpa; fluid, gas; temperature, 169 °F and one closure cycle.

From the proppants baselines: 30/50 Atlas PRC, Bagder Sand, Brady Sand, ValueProp, EconoProp and Sinterball; 40/70 Atlas PRC, Bagder Sand, Brady Sand, CarboProp and EconoProp; 100 mesh White Frac 100 Mesh, InterProp-H Ceramic 35/140 and Badger Sand 70/140, were selected proppants with the best conductivity baselines by type and with low densities. The proppants have a critical pressure above the in-situ stress expected, 5642 psi, assuring that width loss experimented by the fracture is due to embedment. Table 1 records the properties of the chosen proppants, which comes from the Predict-K v.13.1.

Table 1. Physical properties of 30/50, 40/70 and 100 proppants mesh

Property	EconoProp 40/70	EconoProp 30/50	InterProp-H Ceramic 35/140
Type	Low-density Ceramic	Low-density Ceramic	Medium-density Ceramic
Solubility in Acid (wt. %)	-	1.7	2.5
Bulk Density (g/cc)	-	16.005	-
Critical Stress (psi)	13 255.86	11 259.81	10 519.74
Apparent Specific Gravity	2.7	2.683	3.2
Sphericity	0.85	0.9	0.7
Roundness	0.76	0.9	0.7
Turbidity	50	50	-
Porosity (fraction)	0.4079	0.3923	0.4051
Average Diameter (in)	0.012034	0.0204	0.01077

The fracture width decrease can be simulated by compaction. *Equation 10* relates permeability and porosity multipliers to a variable compaction for IMEX. *Equations 11* and *12* establish porosity and permeability as a function of multipliers.

$$Permul = [Pormul]^{m2} \times \left[\frac{\left(\frac{1}{Pori} - 1\right)}{\left(\frac{1}{Pori} - Pormul\right)} \right]^2 \quad (10)$$

$$Por(P) = Pori * Pormul(P) \quad (11)$$

$$Per(P) = Peri * Permul(P) \quad (12)$$

Effective Stress and Multipliers. Cui *et al.* (2014) indicates the relation of minimum horizontal stress and proppant contact pressure where depletion causes increase in contact/closure stress. Montgomery and Steanson (1983) connect fracture gradient and producing bottomhole pressure, in the presence of depletion, both gradient and pressure diminish, but to different rates. Regarding this, in the *Equation 13* all its parameters are unsteady.

$$P_c(t) + P_f(t) = \sigma(t) \quad (13)$$

Once a well is stimulated and open to production, it appears the time dependence. Under these circumstances, $\sigma(0) \leq P_f(0)$ is the initial fracking process or before the treatment and $\sigma(t) > P_f(t)$, final stage or after fracking. Only in the latter case, it can be presented material deformation and proppant embedment (Gao et al, 2013).

To facilitate lecture, the effective parameters are changed in nomenclature leaving: $P_c(t) = P_{ce}$, effective cloussre/contact pressure; $P_f(t) = P_{fe}$, effective fluid pressure (inside the fractures or grid representing a real fracture) and $\sigma(t) = \sigma_e$, the effective minimum horizontal stress.

With an effective horizontal stress of 5642 [psi] for an 8060 [ft] depth. With a BHP of 535 [psi] and an initial reservoir pressure, Pi = 5024 [psi]; regarding the σ_e constant, it is derived the *Equation 14*, which has $618 \leq P_{ce} \leq 5107$ in psi as constraint pressures.

$$P_{ce} = 5642 - P_{fe} \quad (14)$$

With the permeability baselines of the three proppant selected were generated values of Pfe with the closure pressure for each permeability value. Afterwards, it is consider only one proppant type in the fractures and that the conductivity reached 1 [md*ft], when there are not applied stresses $P_{fe} = 5642\ psi \leftrightarrow P_{ce} = 0\ psi$. Now, with the baseline trends and the maximum permeability value in the pressure Pfe are found the permeability multipliers. Porosity multipliers are taken from the roots of the *Equation 10* for the permeability multipliers and a value of unconsolidated sand m2 = 3.5 (Espinoza, 1983), likewise proppants inside a fracture.

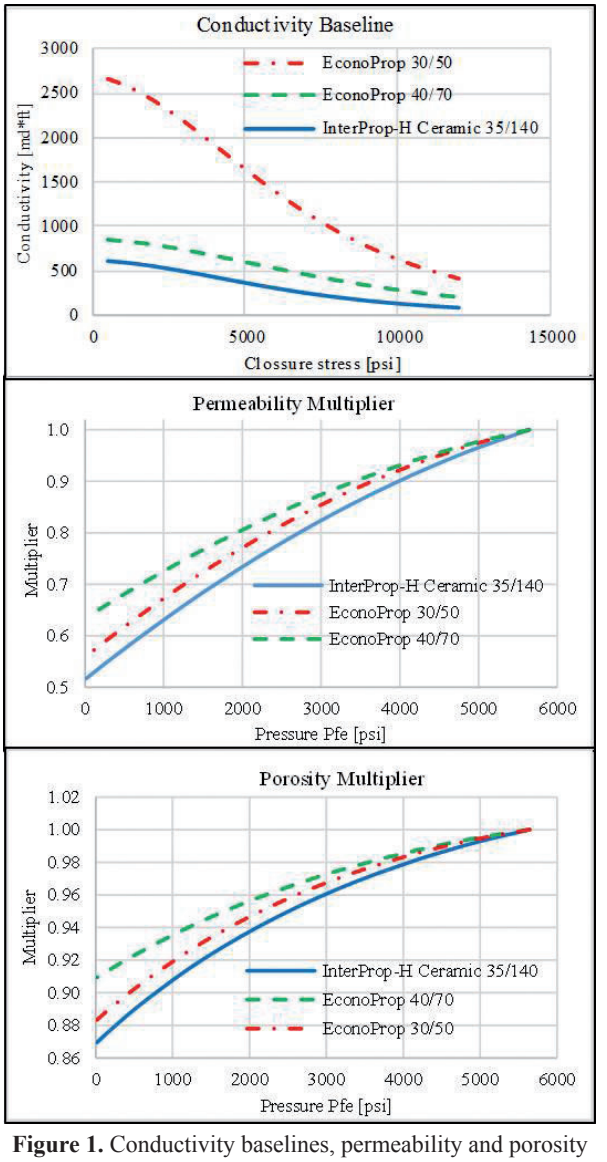

Figure 1. Conductivity baselines, permeability and porosity multipliers
Fuente: Los autores

Simulation Model. ADK-LG-LR (Double Permeability-Logarithmic Grid-Local Refinement) model is used to replicate a base case of reservoir shale and implement the proppant geomechanics. The double permeability model allows to include the natural fractures effects on production, the local logarithmic refinement close to

the fractures lets to evaluate pressure drops accurately. The Table 2 records reservoir properties for a base case of Marcellus Shale, some properties from Yu and Sepehrnoori (2013b) and others modified for this work. The *Equations 15* and *16* define effective properties of permeability and porosity. These adjust the seudofracture flow on the simulator reproducing a real fracture flow. For the embedded fractures the seudofracture has a wide of 1(ft) and a correction of the beta non-darcy flow of 10, to correct flow turbulence in the gas. Inside the natural fractures the spacing is the same found in Marcellus Shale (Ciezobka & Salehi, 2013) and a fracture width of 0.05 (mm) (King, 2010).

$$K_{feff} = \frac{W_{fr} L_{fr}}{W_{fm} L_{fm}} K_f \quad (15)$$

$$\phi_{feff} = \frac{W_{fr} L_{fr} H_{fr}}{W_{fm} L_{fm} H_{fm}} \phi_f \quad (16)$$

Table 2. Reservoir Properties

Reservoir Parameter	Value	Fracture Properties			
Dimensions (ft)	3 800x1 200x173	Explicit (embedded fractures)	Value	Implicit (natural fractures)	Value
Depth TVD (ft)	8 060	Horizontal Well Length (ft)	1 284.4	Horizontal Spacing I and J (ft)	46
Initial Pressure (psi)	5 024	Hydraulic Fractures Number	12	Effective Permeability (mD*ft)	1.46E-06
In-situ Stress (psi)	5 642	Fracture Conductivity (mD*ft)	1	Effective Porosity (fraction)	5.37E-06
Temperature (°F)	169	Fracture Width (ft)	0.01		
Initial Gas Saturation (fraction)	0.7	Fracture Half-Lenght (ft)	400		
Gas Gravity (fraction)	0.5726	Fracture Heigh (ft)	173		
Total Rock Compressibility (1/psi)	3E-06	Horizontal Spacing I (ft)	116.67		
Matrix Permeability (mD)	0.0001	Horizontal Spacing J (ft)	114.2857		
Matrix Porosity (fraction)	0.046				

The rock and fluid properties are shown in the Table 3. The fluid for the reservoir is according to the composition given by Elamin, Fathi and Ameri (2013), who simulated a shale gas reservoir of Marcellus Shale. From that were generated the data needed for simulating with WINPROP: pressure-temperature, volumetric formation factor, gas viscosity and compressibility factor Z. With reference to relative permeability curves, these can vary widely in shale rock conditions and more with confining stresses (Nagarajan, Honarpour & Arasteh, 2013), there is little core information, and measuring properties is a challenge. Nevertheless, with conventional rock information is possible to establish applicable ranges to shale rock (Silseth, 2015), modifying the endpoints given by Silseth (2015), were established the endpoint for the studied case.

History matching result are shown in the Figure 2, this was done to 9 months and are above in the figure, the results of thirty years of simulation are in the left-inferior part, and the location of fractures in the reservoir in the right-inferior part (CMG IMEX v.14.10).

Table 3. Rock and fluid properties

Component	Molar Fraction	Endpoint Keyword	Value
CO2	0.0131	SWCON	0.3
N2	0.0088	SWCRIT	0.3
C1	0.8168	SGCON	0.1
C2	0.0579	SGCRIT	0.1
C3	0.0415	KRWIRO	1
IC4	0.0117	KRGCL	1
NC4	0.0162	Nw	2.5
iC5	0.004	Ng	2
nC5	0.0032		
C6	0.0057		
C7	0.0211		

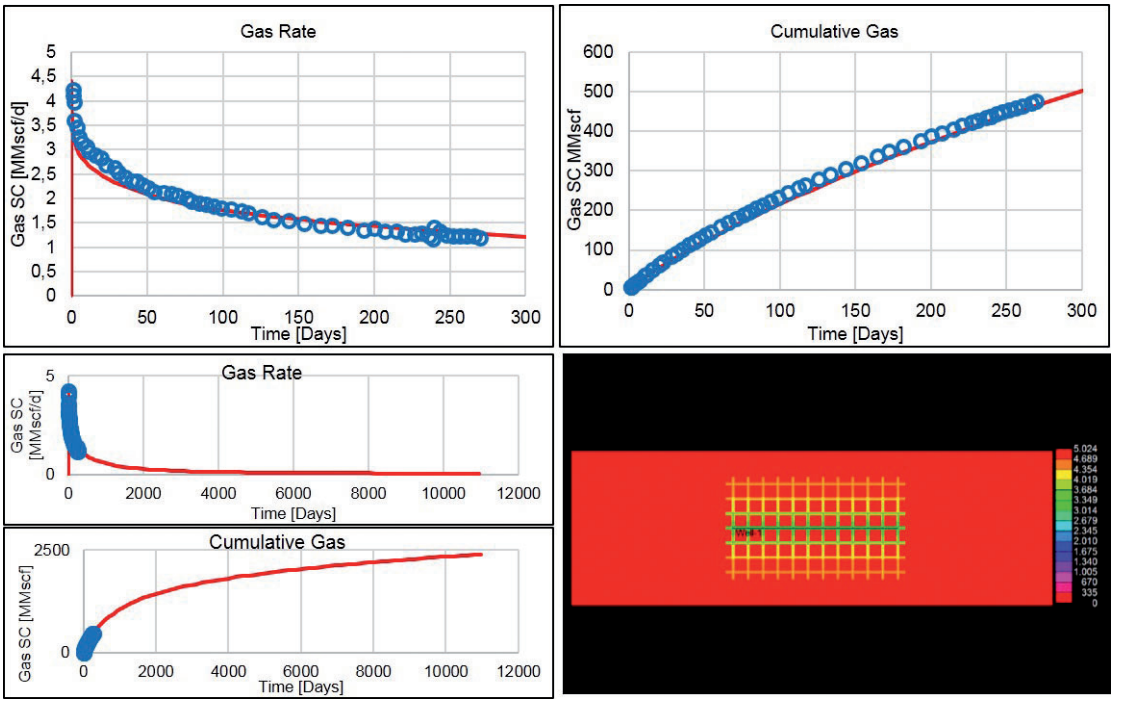

Figure 2. History matching base case: Gas Rate, Cumulative Gas and fractures to 50 days (CMG. Result 3D v.14.10)

4. RESULTS

According to Martins et al. (1992) the effective conductivity (kf*bfe) [md*ft] is proportional to proppant coverage, gas rate and the non-darcy flow; relating the production of each case and the base with the initial conductivity can be obtained the resulting conductivity in the *Equation 17*.

$$C_i = \frac{Q_i}{Q_b} C_0 \tag{17}$$

In the same form as in the *Equation* 17, the resulting width due to embedment is found by the volume ratios of fractures and the initial width in the *Equation 18*.

$$W_i = \frac{VP_i}{VP_b} W_0 \tag{18}$$

In the Figure 3, it can be appreciated the results of simulations. It can be seen in the upper part of the figure the conductivity curves.

In the Figure 3, left-above shows how the major conductivity drop is presented in the first simulation years. When the simulation time reached 0.4 years, the conductivity loss of proppants was: 4.26 %, for 30/50 mesh; 3.84%, 40/70 and 5.09% the 35/140 proppant. From this point is appreciable a decrease in the loss rate, at the end of the simulation time the width shrinkage was: 5.65%, 4.64% and 6.48% for the 30/50, 40/70 and 35/140 proppants, correspondingly. Based upon these results, it can be concluded that the best performance was held by the EconoProp 40/70 proppant through time.

In the Figure 3, right-above is shown conductivities versus effective closure stress reached in the simulation time. At the end of the simulation, the approximate pressure is 4342 psi. Half of the final pressure, 2 171 psi, has a conductivity decrease for the 30/50 proppant of 3.94%, 40/70 of 3.67% and for the 35/140 of 4.82%. As the conductivities were obtained by flow rates ratios, the initial pressures are not reliable as the values after stabilisation.

Fracture width results versus time and pressure can be seen in the Figure 4. In this figure, the fracture width decrease is steady over time and pressure. Initial reduction was: 1.99 %, 3050; 1.93%, 40/70 and 2.16% for the 35/140 proppant. At the end of the simulation, width loss values moved to 7.61%, 6.24%, and 8.61% for the EconProp 30/50, 40/70 proppants and the InterProp-H Ceramic 35/140 proppant.

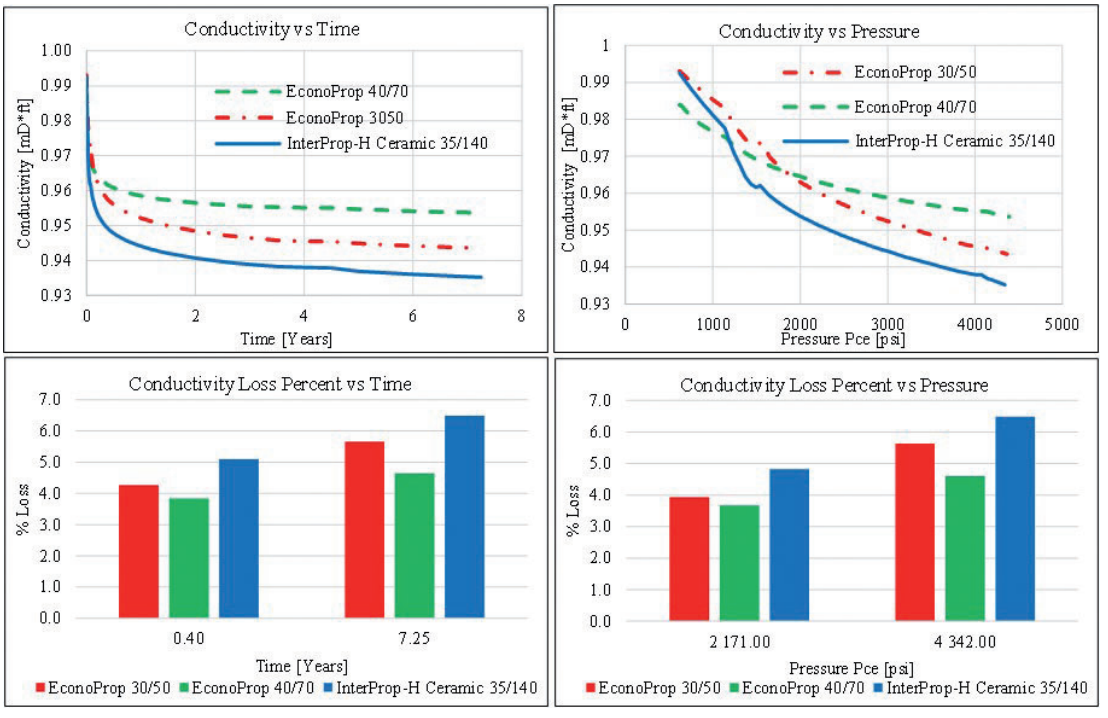

Figure 3. Conductivity vs. time and pressure, percentage of conductivity loss

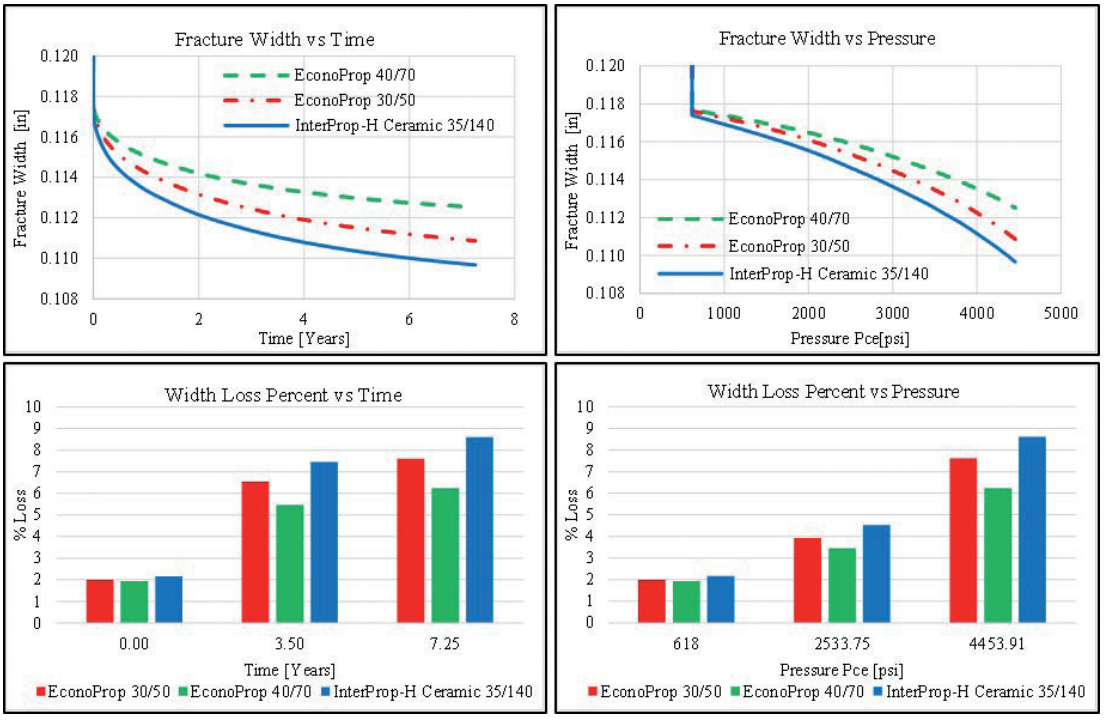

Figure 4. Width vs. time and pressure, percentage of width loss

The equation to model adsorption in IMEX is the *Equation 19*, the Langmuir equation (Yu, Sepehrnoori & Patzek, 2014), with a VL = 500 SCF/Ton (Langmuir Volume) and a PL = 500 psi (Langmuir Pressure) for this approach. Desorption and geomechanics impacts on recovery are quantified by the *Equation 20* (Yu et al., 2014), where Qiref is the reference cumulative gas to a simulation time and Qiv is the cumulative gas of each scenario. The Figure 5 illustrates cumulative gas curves to 30.5 years and their EUR variation (Estimated Ultimate Recovery).

$$G_{ad} = \frac{V_L P}{P+P_L} \tag{19}$$

$$EUR\ Variation = \frac{Q_{iv} - Q_{iref}}{Q_{iv}} \tag{20}$$

In the Figure 5 the four first bars evaluate EUR variation with desorption in relation to the base case without desorption, the last three bars refer to the geomechanics impacts on proppants in the base case including desorption. In the case "bs-b", base with desorption with respect to the base with no desorption (no geomechanics), desorption contributes 0.2386 in the total EUR. In this figure the geomechanics of the EconoProp 40/70 proppant has the best performance, with a desorption contribution in relation with the case lacking desorption of 0.1988 in the EUR and with the minimal decrease: 0.0523 in the EUR, regarding the base case with desorption (isolation of geomechanics effect).

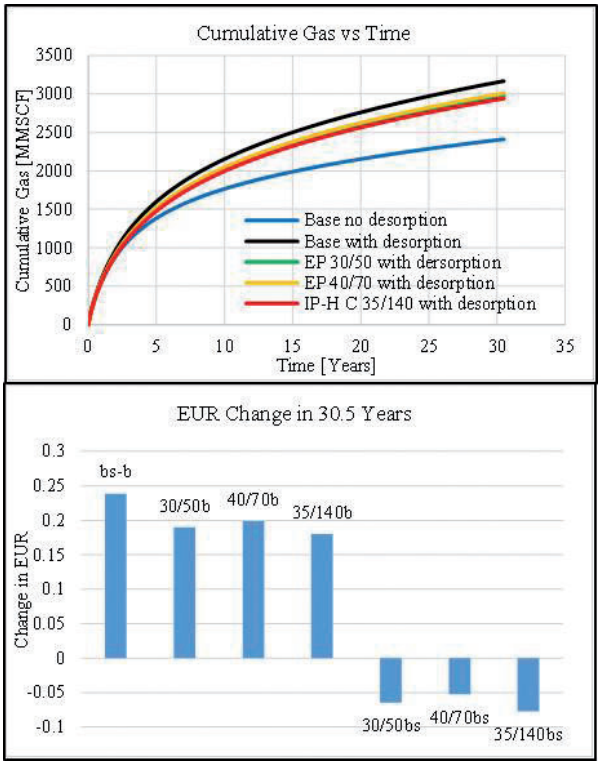

Figure 5. Cumulative Gas and EUR variation to 30.5

5. RESULTS ANALYSIS

A comparison of the simulations results, with some of the models showed and the Predict K are summarised in the Figure 6. The parameters utilised are assembled in the Table 4, proppants Elastic Module and Poisson Ratio according to Chaitanya, M. (2012).

In the Figure 6, the 30/50 proppant width was contrasted with fracture width values obtained according to embedment values reported by Alrahami and Sundberg (2012). The embedment values selected to compare came from a formation with a 33% clay content, Marcellus Shale has an average clay content near 32% (Wang & Carr, 2013). The proppant properties of Alrahami and Sundberg (2012) are similar to the 30/50 proppant in this work, the fracture width values are comparable with the Gao et al. (2013) model results for the same proppant mesh, and it has similarities with the IMEX results. It is important to mention that the clay percentage does not completely define embedment, as it was indicated in the properties section.

Table 4. Parameters of embedment models

Huitt & McGlohtlin 1958			
B	0.000045		
m	1		
K	1		
Mesh	D1 (mm)		
35/140	0.273558		
40/70	0.3056636		
30/50	0.51816		
Gao et al 2013 Multilayer			
E1 (Mpa)	259000		
E2 (Mpa)	24131.65		
v1	0.25		
v2	0.25		
K	1		
D2 (mm)	20		
Mesh	D1 (mm)	b0	b1
35/140	0.273558	0.0180	3.6000
40/70	0.3056636	0.0185	2.3800
30/50	0.51816	0.0160	2.9000

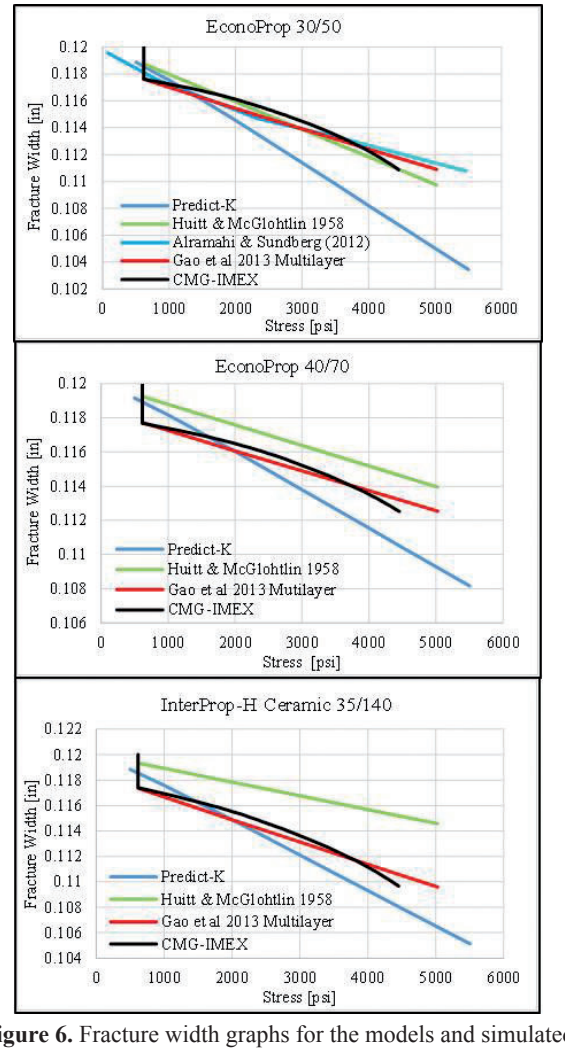

Figure 6. Fracture width graphs for the models and simulated proppants used.

The multilayer values of the Gao et al. (2013) model have the best match because it has adjustment parameters that allow equalisation. With regard to Predict K, this overestimated embedment to stresses above 1500 psi. Under the facts shown, the obtained results of fracture width with the proposed methodology seem to be correct.

6. CONCLUSIONS

Existing models which quantify proppant embedment and conductivity loss have a scarce of complete variables integration, either geomechanics or compositional or geometrics. Nevertheless, the Gao et al *(2013)* multilayer model is versatile because of its correction factors.

Despite of not counting directly on the simulation: mineralogical, geochemical and mechanical rock properties, these influence on the hydraulic fracture performance in shale plays. In the same form, the intrinsic features of the proppant material and fracking fluid composition have an effect on production.

It is possible to replace geomechanics effects in a reservoir with permeability and porosity multipliers. These allow to measure pressure, production, conductivity and width loss by reservoir numerical simulation. Obtaining multipliers have to be a careful task, the type of study to be performed and the proppant material properties have to be regarded.

According to the results in this work, the proppant with the best performance in respect of conductivity and fracture width loss, associated with embedment, is the EconoProp 40/70 amongst the selected to the simulation cases carried out.

Conductivity has not to be related to production and closure stress in a reservoir with drastic changes in its flow, as it occurs in the shale plays. After a flow stabilisation, this can be considered without making significant errors.

ACKNOWLEDGEMENTS

The authors thank to the *Universidad Industrial de Santander* (UIS) for the CMG suite use. The consecution of this work was due to the (*Grupo de Modelamiento de Procesos Hidrocarburos*) (GMPH) acceptance in its group and to allow the development there.

REFERENCES

1. Akrad, O., Miskimins, J., & Prassad, M. (2011) The Effects of Fracturing Fluids on Shale Rock Mechanical Properties and Proppant Embedment. *SPE Annual Technical Conference and Exhibition*, Denver, Colorado, USA. SPE 146658: 7-9.

2. Alexander, T., Baihly, J., Boyer, C., Clark, B., Waters, G., Jochen, V., Le Calvez, J., Lewis, R., Miller, C.,Thaeler, J. & Toelle, B (2011) Shale Gas Revolution. *Oilfield Review*, Autumn 2011; 23(3), 40-55.

3. Alramahi, B. & Sundberg, M. (2012) Proppant Embedment and Conductivity of Hydraulic Fractures in Shales. *48th US Rock Mechanics/Geomechanics Symposium*, Chicago, IL, U.S.A. ARMA 12-291.

4. Chaitanya, M. (2012) Mechanics of Light Weight Proppants: A Discrete Approach. *Ph.D. Dissertation,* Texas A&M University, College Station, Texas, USA, 137pp: 40.

5. Ciezobka, J. & Salehi, I. (2013) Controlled Hydraulic Fracturing of Naturally Fractured Shales – A Case Study in the Marcellus Shale Examining How to Identify and Exploit Natural Fractures. *SPE Unconventional Resources Conference-USA*, Woodlands, Texas, USA. SPE-164524-MS: 4, 5.

6. COMPUTER MODEL GROUP. (2012) User's Guide IMEX Advanced Black Oil/Gas Reservoir Simulator.

7. COMPUTER MODEL GROUP. (2014) CMG Suite, General Release v.14.10.

8. Corapcioglu, H., Miskimins, J. & Prassad, M. (2014) Fracturing Fluid Effects on Young's Modulus and Embedment in the Niobara Formation. *SPE Annual Technical Conference and Exhibition*, Amsterdam, The Netherlands. SPE-170835: 8, 13, 14.

9. CORE LABORATORIES. Program Description and User's Manual. Predict K v.13.1

10. Cui, A., Glover, K. & Wust, R.A.J. (2014) Elastic and plastic mechanical properties of liquid-rich unconventional shales and their implications for hydraulic fracturing and proppant embedment: a case study of the Nordegg Member in Alberta, Canada. *48th US Rock Mechanics/Geomechanics Symposium*, Minneapolis, MN, USA. ARMA 14-7556.

11. Elamin, A., Fathi, E. & Ameri, S. (2013) Simulation of Multicomponent Gas Flow and Condensation in Marcellus Shale Reservoir. *SPE Unconventional Resources Conference-USA*, Woodlands, Texas, USA. SPE-164538-MS: 8.

12. Espinoza, C. (1983) A New Formulation for Numerical Simulation of Compaction, Sensitivity Studies for Steam Injection. *SPE Reservoir Simulation Symposium, San Francisco*, California, USA. SPE-12246-MS.

13. Fredd, C., McConnell, S., Boney, C. & England, K. (2000) Experimental Study of Hydraulic Fracture Conductivity Demonstrates the Benefits of Using Proppants. *2000 SPE Rocky Mountain Regional/Low Permeability Reservoirs Symposium*, Denver, CO, USA. SPE 60326: 6, 14.

14. Gao, Y., SINOPEC Petroleum Exploration & Production Research Institute, Lv, Y., Wang, M., China Pingmei Shenma Group, Li, K., China University of Geosciences (Beijing) & Yangtze University. (2013) New Mathematical Models for Calculating the Proppant Embedment and Conductivity. *International Petroleum Technology Conference*, Beijing, China. IPTC 16410.

15. Guo, J., Liu, Y. (2012) Modeling of Proppant Embedment: Elastic Deformation and Creep Deformation. *SPE International Production and Operations Conference and Exhibition*, Doha, Qatar. SPE 157449: 4, 8.

16. Huitt, J. & McGlothlin, Jr. (1958) The Propping of Fractures in Formations Susceptible to Propping-sand Embedment. *Pacific Coast District, Division of Production*, Los Angeles, California, USA. API-58-115.

17. Kassis, S. & Sondergeld, C. (2010) Fracture Permeability of Gas Shale: Effects of Roughness, Fracture Offset, Proppant, and Effective Stress. *CPS/SPE International Oil & Gas Conference and Exhibition in China*, Beijing, China. SPE 131376: 3, 4, 11.

18. King, G. (2010) Thirty Years of Gas Shale Fracturing: What Have We Learned? *SPE Annual Technical Conference and Exhibition*, Florence, Italy. SPE 133456: 8, 17.

19. Lacy, L., Rickards, A. & Bilden, D. (1998) Fracture

Width and Embedment Testing in Soft Reservoir Sandstone. *SPE Drilling & Completion*, 13(01), 25-29: 27, 28.

20. Lacy, L., Rickards, A. & Ali, S. (1997) Embedment and Fracture Conductivity in Soft Formations Associated with HEC, Borate and Water-Based Fracture Designs. *1997 SPE Annual Technical Conference and Exhibition*, San Antonio, Texas, USA. SPE 38590.

21. Martins, J., Leung, K., Jackson, M., Stewart, D. & Carr, A. (1992) Tip Screenout Fracturing Applied to the Ravenspurn South Gas Field Development. *SPE Production Engineering*, 7(3), 252-258: 253.

22. Montgomery, C. & Steanson (1985) Proppant Selection: The Key to Successful Fracture Stimulation. *Journal of Petroleum Technology*, 37(12), 2163-2172: 2165.

23. Nagarajan, N. Honarpour, M. & Arasteh. (2013) Critical Role of Rock and Fluid - Impact on Reservoir Performance on Unconventional Shale Reservoirs. *Unconventional Resources Technology Conference*, Denver, Colorado, USA. SPE-168864-MS: 2.

24. Silseth, J. (2015) Effect of Relative Permeability on History Matching a Permian Basin Oil Well. *M.Sc. Thesis, Department of Petroleum Engineering and Applied Geophysics*, Norwegian University of Science and Technology, Norway, 109pp: 28.

25. Terracina, J., Turner, J., Collins, D. & Spillars. (2012) Proppant Selection and Its Effect on the Results of Fracturing Treatments Performed in Shale Formations. *SPE Annual Technical Conference and Exhibition*, Florence, Italy. SPE 135502: 3.

26. Wang, G. & Carr, R. (2013) Organic-rich Marcellus Shale lithofacies modeling and distribution pattern analysis in the Appalachian Basin. *AAPG Bulletin*, December 2013; 97 (12), 2173-2205: 21181.

27. Yu, W. & Spehrnoori, K. (2013a) Simulation of Gas Desorption and Geomechanics Effects for Unconventional Gas Resources. *SPE Western Regional & AAPG Pacific Section Meeting, 2013 Joint Technical Conference*, Monterrey, California, USA. SPE 165377.

28. Yu, W. & Spehrnoori, K. (2013b) Simulation of Proppant Distribution Effect on Well Performance in Shale Gas Reservoirs. *SPE Unconventional Resources Conference-Canada*, Calgary, Alberta, Canada. SPE 167225.

29. Yu, W., Sepehrnoori, K. Patzek, T. (2014) Evaluation of Gas Adsorption in Marcellus Shale. *SPE Annual Technical Conference and Exhibition*, Amsterdam, The Netherlands. SPE-170801-MS: 3, 10.

NOMENCLATURE

a = Distributed loading radius, mm;
b_0 = Adjustment Parameter, mm;
b_1 = Adjustment Parameter, dimensionless;
B = Characteristic constant of formation, dimensionless;
C_0 = Initial conductivity, md*ft;
C_E = Constant associated with Elastic and Poisson Moduli of spheres 1 and 2, [Mpa]^(-1);
C_i = Conductivity of the studied proppant i, md*ft;
D = Initial fracture aperture, mm;
D_1 = Proppant diameter, mm;
D_2 = Thickness of the coalbed, mm;
dt = Time differential;
E = Rock Elastic Modulus, MPa;
E_1 = Proppant Elastic Modululus (sphere 1), Mpa;
E_2 = Elastic Modulus of the coalbed/formation (spehere 2), Mpa;
G_{ad} = Adsorbed gas, scf/ton;
h = Embedment value, mm;
H_1 = Embedment value due to elastic deformation, mm;
H_2(t) = Embedment value due to creep deformation (viscous-elastic), mm;
H_{fr} = Height of theoretical or real fracture, ft;
H_{fm} = Fracture model height, ft;
K = Distance coefficient, dimensionless;
K_f = Fracture permeability or reference permeability, md;
K_{feff} = Effective permeability, md;
L_{fr} = Length of theoretical or real fracture, ft;
L_{fm} = Fracture model length, ft;
$m1$ = Characteristic constant of formation (Huit & McGlothlin, 1958), dimensionless;
$m2$ = Characteristic constant of formation (IMEX), dimensionless;
P = Pressure, psi;
$P_c(t)$, p = Effective closure stress, Mpa;
P_c = Clossure stress, Mpa;
P_{ce} = Effective closure/contact pressure, psi;
P_{fe} = Fluid pressure inside a fracture or a grid representing a fracture, psi;
Permul = Permeability multiplier, dimensionless;
Permul (P) = Permeability multiplier in function of pressure, dimensionless;

Per (*P*) = Permeability in function of the multpliers and pressure, md;
Peri = Initial permeability, md*ft;
P_L = Langmuir pressure, psi;
Pori = Initial porosity, fraction;
Pormul = Porosity multiplier, dimensionless;
Pormul (*P*) = Porosity multiplier in function of pressure, dimensionless;
Por (*P*) = Porosity in function of the multpliers and pressure, fraction;
Q_b = Cumulative production base case, MMscf;
Q_i = Cumulative production of the studied case i, MMscf;
Q_{iv} = Cumulative production of the studied case i at the final simulation time, MMscf;
Q_{iv} = Cumulative production of reference at the final simulation time, MMscf;
t = Time of stage, t = 0 Elastic, t = 1 Creep, t = n stage of creep; dimensionless;
V_L = Langmuir volume, scf/ton;
VP_b = Base case porous volume, cf;
VP_i = Porous volume of the case i, cf;
W_0 = Initial fracture width, in;
W_i = Fracture width of the case i, in;
W_{fr} = Fracture width teorethical or real, ft;
W_{fm} = Model fracture width, ft;
α = Variation in fracture aperture, mm;
ϕ_f = Fracture porosity or reference porosity, mm;
ϕ_{feff} = Effective porosity, fraction;
β =Proppant deformation, mm;
$\sigma(t)$, σe = Horizontal stress, Mpa, psi;
η_2 = Viscous-elastic coefficient in the second creep stage, Mpa;
v = Formation Poisson ratio, dimensionless;
v_1 = Proppant Poisson ratio (sphere 1), dimensionless;
v_2 = Formation Poisson ratio (sphere 2), dimensionless;

SI METRIC CONVERSIONS FACTORS

ft	x 3.048	*E-01 = m
in	x 2.54	* E+01 = mm
lbm/ft^2	x 4.88243	* E+00 = Kg/m^2
mD*ft	x 3.008 142	*E−04 = mD*m
MMscf	x 2.831 685	*E−02 = Mm3 (standard Millions)
MMscf/d	x 2.863 640	*E−02 = Mm3/d (standard Millions)
psi	x 6.894 757	* E+00= kPa (°F-32) x (9/5) = °C

Recepción: 25 de julio de 2016
Aceptación: 12 de octubre de 2016